

Remote synchronization of amplitudes: a demodulation and interference effect

Ludovico Minati,^{1,2, a)} Luca Faes,^{3,4} Mattia Frasca,⁵ Paweł Oświęcimka,¹ and Stanisław Drożdż^{1,6}

¹⁾ *Complex Systems Theory Department, Institute of Nuclear Physics Polish Academy of Sciences (IFJ-PAN), Kraków, Poland*

²⁾ *Center for Mind/Brain Sciences (CIMEC), University of Trento, Trento, Italy*

³⁾ *Department of Energy, Information Engineering and Mathematical Models (DEIM), University of Palermo, Palermo, Italy*

⁴⁾ *BIOTech, Department of Industrial Engineering, University of Trento, Trento, Italy*

⁵⁾ *Department of Electrical Electronic and Computer Engineering (DIEEI), University of Catania, Catania, Italy*

⁶⁾ *Faculty of Physics, Mathematics and Computer Science, Cracow University of Technology, Kraków, Poland*

(Dated: 3 December 2024)

A form of remote synchronization was recently described wherein amplitude fluctuations across a ring of non-linear electronic oscillators become entrained into structured patterns. Here, the underlying mechanism is finally elucidated. Through numerical simulations of rings having different size and a simplified chain model, as well as experiments involving injection of additive noise hindering the synchronization of individual units, it is demonstrated that the effect emerges from local interactions between each node and its surroundings. The non-linearity is found to have a dual role, supporting chaotic dynamics as well as enabling energy exchange between the lower and higher sidebands of the predominant frequency, which acts as carrier signal in an arrangement resembling standard amplitude modulation. The lower sideband and the demodulated baseband signal spectrally overlap. Remote synchronization arises because of a spatially-dependent phase relationship between them, such that at a certain distance near-complete destructive interference occurs. An information-theoretic account of the network dynamics is provided based on Granger causality with linear and non-linear models, transfer entropy and self-entropy, enabling the investigation of the relationship between information transfer and flow through experiments on the propagation of external perturbations. The results demonstrate a non-trivial mechanism of pattern formation and dynamical interdependence.

A fundamental aim of non-linear science is to understand the collective behavior of units interacting with one another according to a given network of structural connections, possibly but not necessarily reflecting their physical locations. Even though a general theory is missing, it is understood that there are diverse mechanisms through which dynamics can give rise to synchronization patterns having complex features potentially absent in the underlying structural connections. One such mechanism is “remote synchronization”, namely the selective or preferential entrainment between groups of units (e.g., oscillators) that are not structurally connected, as observed for example between neurons in distant brain regions or meteorological processes over different continents. Here, we present an explanation for a peculiar form of remote synchronization, previously discovered in a ring of electronic non-linear oscillators. By means of

^{a)} Author to whom correspondence should be addressed. Electronic addresses: ludovico.minati@ifj.edu.pl and lminati@ieee.org. Tel.: +39 335 486 670. URL: <http://www.lminati.it>.

new experiments and simulations, it is found that remotely-synchronized amplitude fluctuations can arise via an interference effect, which reflects more closely “local” interactions than the collective behavior of the network as a whole. The effect arises in a scenario reminiscent of amplitude modulation, wherein the system non-linearity demodulates the envelope signal. An information-theoretical account of the results is given, exemplifying the potential consequences of linear vs. non-linear model choice and the relationship between the statistical features of intrinsic activity (reflected in the so-called information transfer) and ability to propagate external perturbations (information flow). Some arguments around the generality of the effect are considered.

I. INTRODUCTION

Coupled non-linear oscillators have an extraordinary generative potential with respect to forming synchronization patterns not straightforwardly related to structural connections^{1–9}. While the means through which such patterns can be formed are diverse and difficult to classify univocally, well-known phenomena include cluster synchronization², relay synchronization^{3,4}, formation of chimera states^{5,6} and remote synchronization^{7–9}. The latter, in particular, encompasses heterogeneous mechanisms, which have in common the fact that they lead to pairs or subsets of oscillators becoming synchronized in the absence of direct structural connections, and more strongly than any other intermediate units potentially acting as dynamical relays. For example, in a chain of four sequentially numbered oscillators, nodes 1 and 4 are said to be remotely synchronized if they are more strongly synchronized with each other than with nodes 2 and 3, which by virtue of the coupling necessarily act as dynamical relays.

Known instances of remote synchronization may be broadly grouped according to whether they involve large parametric mismatches^{7,8} or identical nodes^{9,10}. As regards the first group, the term remote synchronization has been used to denote the onset of phase synchronization among the outer nodes of a star network of periodic oscillators wherein the central hub has mismatched natural oscillation frequency and is not synchronized with them⁷. This phenomenon partially overlaps that of relay synchronization, which is observed for chaotic oscillators and manifests as complete synchronization of the outer nodes mediated by the central one which is synchronized with them in a weaker sense, such as with a lag³ or a generalized relationship¹¹. Notably, both phenomena are also found in complex random topologies beyond the simple motifs where they have first been observed^{4,8}. As regards the second group, symmetries in the structural connections engender the emergence of remotely-synchronized node subsets, and the term remote synchronization has been used to refer to the formation of node subsets having coherent phase or common trajectory, and interconnected via other nodes involving either a lag⁹ or completely incoherent¹⁰ dynamics. A peculiar form of remote synchronization was recently elicited in a ring network of oscillators involving small parametric mismatches. In this system, remote synchronization emerges for amplitude fluctuations concomitantly with underlying global phase synchronization, and leads to the appearance of patterns having complex features such as small-world topology. In the initial study¹², the effect was extensively demonstrated through simulations and experiments involving a network of reconfigurable non-linear electronic oscillators (field programmable analog arrays, FPAAs), but an understanding of the underlying mechanism was not attained. It was merely indicated that it involves the formation of complex interdependencies between coupled units, visible solely to suitably generalized synchronization measures.

Here, a detailed account of the underlying mechanism is finally given. After a description of the system structure and observed synchronization effect, the interactions between oscillators are revisited from a causality perspective, and new experiments involving external perturbation with white noise and sinc pulses are reported. Alongside simulations

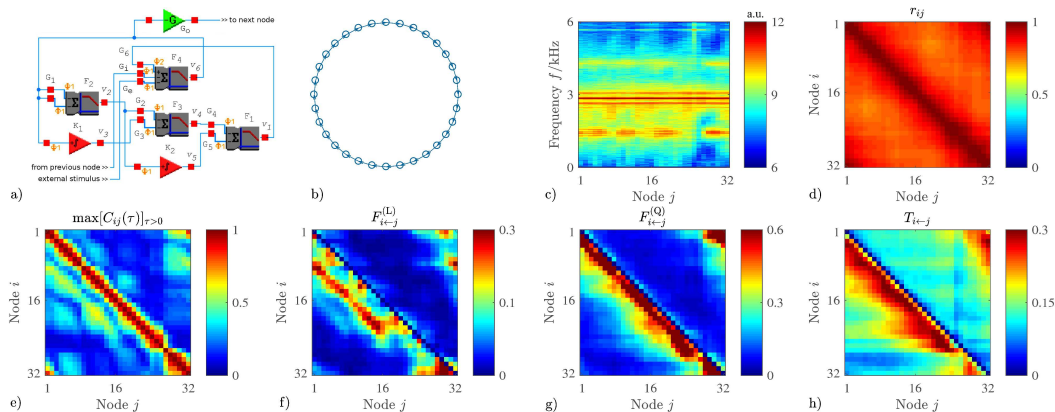


FIG. 1. Chaotic oscillator network, with corresponding frequency spectra, synchronization and causality matrices. a) Circuit instantiated at each node, consisting of a ring oscillator to which two integrators are superimposed. b) Network comprising 32 such circuits forming a ring via master-slave coupling. c) Spectrogram depicting the Fourier log-amplitudes across the nodes. d) Phase coherence calculated for a representative, experimentally-measured signal. e) Maximum positive-lag cross-correlation coefficient for the signal envelope (amplitude fluctuations, thereafter referred to as amplitude synchronization). f) Corresponding Granger causality according to the linear model. g) Granger causality according to a model including quadratic terms and cross-terms. h) Transfer entropy, calculated with a model-free approach. Raw signals from Ref. 12. See Sections II and III for detailed description.

of different size rings and a simplified chain model, these unequivocally demonstrate that the effect, rather than representing global collective behavior of the network, emerges from local interactions between each node and its surroundings. After confirming chaoticity and the relevance of parametric mismatches, the underlying demodulation and interference mechanism is revealed, informing a revised, ad-hoc causality model which is applied to the initial experimental data.

II. SYSTEM STRUCTURE AND DYNAMICS

Each individual oscillator consists of a ring of three composite stages, which implement gain, summation and low-pass filtering, and of two integrators whose outputs enter different points of the ring (Fig. 1a). This structure effectively forms a sort of ring oscillator, and was developed specifically since it supports rich dynamics and at the same time is suitable for physical deployment using a single FPAA device¹². The oscillator dynamics are governed by the following system

$$\begin{cases} \frac{dv_1}{dt} = \Gamma(2\pi F_1(G_4 v_4 + G_5 v_5 - v_1), v_1) \\ \frac{dv_2}{dt} = \Gamma(2\pi F_2(G_1 v_6 - v_2), v_2) \\ \frac{dv_3}{dt} = \Gamma(K_1 v_6, v_3) \\ \frac{dv_4}{dt} = \Gamma(2\pi F_3(G_2 v_2 + G_3 v_3 - v_4), v_4) \\ \frac{dv_5}{dt} = \Gamma(K_2 v_2, v_5) \\ \frac{dv_6}{dt} = \Gamma(2\pi F_4(G_6 v_1 + G_i v_i + G_e v_e - v_6), v_6) \end{cases} \quad (1)$$

wherein the only non-linearity is the function $\Gamma(x, y)$, which represents an approximation of saturation effects due to finite voltage swing $V_s = 4$ according to

$$\Gamma(x, y) = R(x)H(V_s - y) - R(-x)H(V_s + y) \quad (2)$$

where the Heaviside function $H(x) = 1$ for $x > 0$, 0 for $x \leq 0$ and the ramp function $R(x) = xH(x)$. The oscillator output voltage corresponds to $v_o = G_o v_6$, where $G_o = -0.4$. Each oscillator receives as input the signal, denoted as v_i , from the preceding node on a unidirectionally (e.g., master-slave) coupled ring of 32 oscillators (Fig. 1b); in addition, v_e denotes the external perturbation voltage which was applied during the experiments reported in Section IV. As clarified below, a strongly periodic signal acting as a ‘‘carrier’’ is generated, and features a phase lead in the coupling direction engendered by the integrative dynamics; concomitantly, large amplitude fluctuations emerge, for the propagation of which a lag is observed in the direction of coupling.

Unless otherwise noted, we set $G_1 = -3.6$, $G_2 = -3.12$, $G_3 = -0.5$, $G_4 = -3.08$, $G_5 = -0.71$, $G_6 = 0.132$, $F_1 = F_2 = F_3 = 2$ kHz, $F_4 = 100$ kHz, $K_1 = 3.67K_2 = 0.11 \mu\text{s}^{-1}$, $G_i = -1.44$, $G_e = 0$ and $V_s = 4$ V, corresponding to the case shown in Fig. 7a of Ref. 12, and used the corresponding publicly-available experimental time-series for analyses. The gains G_6 and G_i respectively control the internal loop gain and coupling strength of each oscillator with the preceding one on the ring, and act as the main control parameters, whereas the integration constant K_1 acts an additional control parameter¹².

Due to reasons related to construction of the physical system, there are unavoidable tolerances in the realization of these parameters, which are on the order of 0.5%. The values indicated above therefore actually prescribe the nominal values for the parameters. Given a parameter P having average $\langle P \rangle$ (representing G_1 , G_2 etc.), tolerances can be represented by extracting individual realizations from a uniform distribution of the form

$$f(x) = \begin{cases} \frac{1}{2\xi\langle P \rangle} & \text{for } \langle P \rangle(1 - \xi) \leq x \leq \langle P \rangle(1 + \xi) \\ 0 & \text{otherwise} \end{cases} \quad (3)$$

where $\xi = 0.005$.

The frequency spectrum features three broad but clearly-distinct peaks: a prominent central peak at $f_c \approx 2.8$ kHz (here appearing split, plausibly due to the parametric mismatches) and two weaker peaks at $f_l = f_c/2 \approx 1.4$ kHz and $f_h = f_l + f_c \approx 4.2$ kHz, having the appearance of its lower and higher sidebands (Fig. 1c); faint resonances are also found at $f_l + f_h \approx 5.6$ kHz and $f_c + f_h \approx 7.1$ kHz (data not shown). The lower sideband reflects amplitude fluctuations, and specifically the relationship $f_l = f_c/2$ is verified because of strong anti-persistence, having Hurst exponents¹³ $H_{\text{max}} = 0.15 \pm 0.00$ and $H_{\text{min}} = 0.26 \pm 0.00$ for the maxima and minima respectively, stemming from an underlying period-doubling bifurcation. The higher sideband represents the mirror frequency of the lower one. As elucidated in Section VII, a phenomenon of demodulation via envelope detection and subsequent interference leads to spatial fluctuations of the lower sideband amplitude resembling a diffraction pattern, which are closely related to the remote synchronization effect (Fig. 1c).

As in Ref. 12, the instantaneous phase $\varphi_i(t)$ and amplitude $A_i(t)$ (i.e., envelope) of the output signal $v_i(t)$ of each oscillator i were calculated via the analytic signal according to

$$v_i(t) + i\hat{v}_i(t) = A_i(t)e^{i\varphi_i(t)} \quad (4)$$

where \hat{v}_i is the Hilbert transform of $v_i(t)$

$$\hat{v}_i(t) = \frac{1}{\pi} \text{p.v.} \left[\int_{-\infty}^{\infty} \frac{v_i(\tau)}{t - \tau} d\tau \right] \quad (5)$$

and where p.v. denotes the Cauchy principal value of the integral¹⁴. Phase coherence was measured with

$$r_{ij} = |\langle e^{i[\varphi_i(t) - \varphi_j(t)]} \rangle| \quad (6)$$

and revealed global, albeit imperfect, phase synchronization (Fig. 1d). Amplitude synchronization was measured in terms of the maximum cross-correlation coefficient of $A_i(t)$ for positive lags and revealed a pattern wherein, besides incomplete regularity due to the parametric heterogeneity, the predominant feature was that, moving away from a given node, synchronization initially decayed then increased again peaking at a distance $d = i - j \approx 8$, and eventually vanished (Fig. 1e). As structural coupling on the ring is only between first neighbors, this represents a form of remote synchronization.

III. LINEAR, QUADRATIC AND MODEL-FREE CAUSALITY ANALYSES

Synchronization measures such as phase coherence and the maximum cross-correlation coefficient are symmetric, i.e. equal in the $i \rightarrow j$ and $j \rightarrow i$ directions, and therefore inherently incapable of detecting causality between coupled units in an observational framework (referred to as *information transfer*); this is exemplified by two identical oscillators having the same starting conditions, which can remain perfectly synchronized in the absence of any energy exchange. Even observation of temporal precedence via time-lagged measures is inadequate for establishing causality, in that it does not distinguish the information actually exchanged by the units from that only shared in response to common inputs or past history^{15,16}. These issues are of particular concern since in the present system the oscillators are nearly identical, i.e. $\xi \ll 1$, and the connectivity is closed-loop.

For correctly inferring causality between two coupled units in an observational framework, meaning without probing the system response to an external perturbation, one needs to quantify the amount of information shared between the past states of the driver and the present state of the target, which is not accounted for the past states of the target. This is essential because deterministic systems such as chaotic oscillators can generate autocorrelated activity, and therefore store significant amounts of information which confounds the relationship between information transfer and synchronization measures^{17,18}.

We therefore investigated whether in the present system remote synchronization truly represents remote information transfer, by applying Granger causality computed in its parametric formulation based on linear and nonlinear regression models^{19,20}, and in its nonparametric formulation directly expressed in information-theoretic terms and known as transfer entropy^{15,16}. These measures of information transfer reflect causality according to a probabilistic notion, positing that activity in a node j is Granger-causal to activity in another node i if and only if knowledge of the past of node j improves prediction of the present of node i above and beyond the predictability yielded by knowledge of the past of node i itself¹⁹. Since in the present system remote synchronization is observed for signal envelopes, for these analyses we represented dynamics with the instantaneous amplitudes, i.e. $y_i(t) = A_i(t)$.

First, causality was investigated by performing a linear regression of the present state of each node i , $y_i(t)$, given its past state $Y_i^P(t) = [y_i(t - \tau), \dots, y_i(t - p\tau)]$, yielding prediction error $e_{i|i}(t) = y_i(t) - \mathbb{E}[y_i(t)|Y_i^P(t)]$, and given the past states of both i and j , $Y_{i,j}^P(t) = [Y_i^P(t), Y_j^P(t)]$, yielding prediction error $e_{i|i,j}(t) = y_i(t) - \mathbb{E}[y_i(t)|Y_{i,j}^P(t)]$. The prediction error variances given by these two regressions, $\lambda_{i|i} = \mathbb{E}[e_{i|i}^2]$ and $\lambda_{i|i,j} = \mathbb{E}[e_{i|i,j}^2]$, were combined to yield the Granger causality from node j to node i ²⁰

$$F_{i \leftarrow j}^{(L)} = \log \frac{\lambda_{i|i}}{\lambda_{i|i,j}}. \quad (7)$$

In this and the subsequent analyses, the lag τ was set to 0.18 ms, corresponding to the first local minimum of the time-delayed mutual information, taken as an empirical estimator of the time-scale of dynamics²¹. Determination of model order p was more problematic, given that the Akaike and Bayesian Information Criteria (AIC, BIC)²² both decreased monotonically up to $p = 20$, indicating that a linear model does not fully describe the dynamics; $p = 16$ was chosen as a compromise sufficiently covering past history without excessively elevating model order, and $p = 8$ or 32 yielded comparable results.

As shown in Fig. 1f, the resulting pattern closely tracked the maximum cross-correlation for positive lags (Fig. 1e), confirming that insofar as a linear model is concerned, in this system remote synchronization reflects remote information transfer which, as expected given the unidirectional coupling (Fig. 1b), was strongly asymmetric.

However, it has previously been established that a linear model is insufficient to capture the dynamics of this system¹². To overcome this limitation while retaining a parametric approach, the model was extended to account for non-linear Granger-causal influences by including quadratic terms (e.g., $y_i^2(t - m\tau)$) and cross-terms (e.g., $y_i(t - m\tau)y_i(t - n\tau)$ for $m \neq n$) into the regressors $Y_i^p(t)$ and $Y_{i,j}^p(t)$ ²³. The resulting nonlinear measure is referred to as $F_{i \leftarrow j}^{(Q)}$. For consistency, the τ and p settings were retained.

As shown in Fig. 1g, we observed $F_{i \leftarrow j}^{(Q)} \gg F_{i \leftarrow j}^{(L)}$, and the causality pattern according to $F_{i \leftarrow j}^{(Q)}$ was substantially different from that of $F_{i \leftarrow j}^{(L)}$ in that it featured a gradual, monotonic decay of information transfer with respect to distance d . This result provides an initial indication that causal interdependence in this system is actually not remote, simply it is “hidden” to the linear model for an intermediate range of distances, where phase coherence dips but a more complex relationship is maintained.

A more general measure of information transfer, namely transfer entropy, can be defined without recourse to any model, directly in probabilistic terms as a conditional mutual information¹⁵, according to

$$T_{i \leftarrow j} = I(y_i(t); Y_j^p(t) | Y_i^p(t)) \quad (8)$$

and practically computed by estimating its four entropy terms¹⁶

$$\begin{aligned} I(y_i(t); Y_j^p(t) | Y_i^p(t)) = & H(y_i(t), Y_i^p(t)) - H(Y_i^p(t)) - \\ & H(y_i(t), Y_{i,j}^p(t)) + H(Y_{i,j}^p(t)) \end{aligned} \quad (9)$$

where $H(Y|X)$ represents the entropy of Y conditioned on X . Here, $T_{i \leftarrow j}$ was estimated with the nearest-neighbor method, implemented with a distance projection which compensates for the different biases of the individual entropy estimates^{24,25}. We reduced the order to $p = 8$ since for higher settings $T_{i \leftarrow j}$ dropped considerably due to the excessive estimation bias induced by the curse of dimensionality.

As shown in Fig. 1h, the pattern closely resembled that obtained from the non-linear Granger causality model, approaching the relationship expected for Gaussian variables²⁶ $T_{i \leftarrow j} \approx F_{i \leftarrow j}^{(Q)}/2$, suggesting that the proposed non-linear model already captures the dynamics adequately, and moreover confirming the results obtained with a rank-based measure of generalized synchronization in the initial study¹². As will become clear in Section VIII, this result can be recovered with an ad-hoc linear Granger model explicitly representing the overlapped low-frequency signal and demodulated baseband signal.

IV. PERTURBATION BY WHITE NOISE AND SINC PULSES

The observational framework considered thus far does not yield insight into whether remote synchronization is underpinned by local interaction between each node and its surroundings, a global phenomenon such as a collective oscillation mode, or perhaps a combination between the two. To address this issue, it is necessary to conduct new experiments involving external interventions, i.e. perturbing the intrinsic activity with unrelated stimuli^{27,28}.

It is well established that, by causing dispersion in phase space, additive noise perturbing individual units can exert a strong desynchronizing effect in coupled systems, even when its intensity is relatively limited compared to that of the intrinsic activity^{29,30}. Further, as the present oscillators can inherently not be entrained by a stochastic signal, upon injecting noise at a certain location on the ring its amplitude will gradually decrease in the direction of the structural coupling, and will be minimal at the node preceding the injection site.

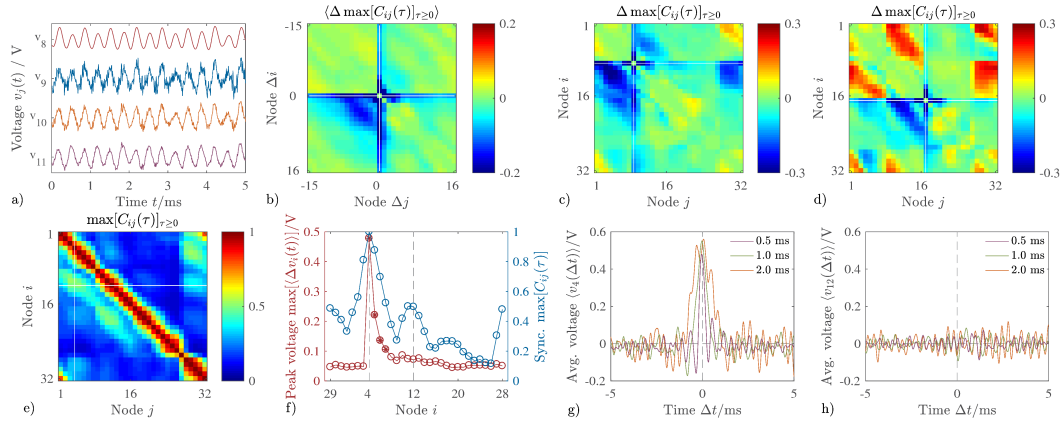


FIG. 2. Experiments applying external perturbations. a) Representative signals measured before (v_8), at (v_9) and after (v_{10} , v_{11}) a site where high-intensity white noise was injected. b) Change in amplitude synchronization (maximum cross-correlation coefficient) due to noise injection, averaged across all nodes while rotating the ring to center the injection site $\Delta i = \Delta j = 0$. c) and d) Corresponding examples for noise injection at nodes $j = 9, 17$. e) Amplitude synchronization averaged while injecting low-amplitude sinc pulses at node $j = 4$, showing negligible difference compared to Fig. 1e. f) Monotonic decay of the sinc pulse amplitude with distance along the ring (red, stars indicate statistically-significant signal detected), with concomitant remote synchronization of intrinsic activity at node $j = 12$ (blue). g) and h) Time-locked signal average calculated for the injection site and the site corresponding to the remote synchronization peak, $j = 4, 12$. See Section IV for detailed description.

It is therefore possible to use externally-generated noise as a means of inducing localized desynchronization.

Experiments were performed setting $G_6 = 0.12$, $G_i = -1.56$, $K_1 = 0.121 \mu\text{s}^{-1}$ and $G_e = 10$, and introducing Gaussian white noise from an external arbitrary waveform generator (HP33120A; Agilent Inc., Santa Clara CA, USA), with $\sigma_{\text{noise}} \approx 300 \text{ mV}$ and $\sigma_{\text{signal}}/\sigma_{\text{noise}} \approx 1.5$. As expected, the relative noise intensity rapidly decreased over few steps after the injection site (Fig. 2a). Desynchronization manifested itself primarily through obliteration of remote synchronization between the nodes before and after the injection site, a result which was well-evident both when averaging the effect over all possible injection sites (Fig. 2b) and when considering individual examples (Figs. 2c,d). Since the difference was primarily confined to the nodes in the vicinity of the injection site, this result provides an initial indication that remote synchronization is a “local” effect, i.e. does not reflect an emergent property of the collective dynamics of the ring as a whole but contrariwise represents some sort of “transformation” which is at least partially reversed after a certain number of steps from a starting to an end node. As will become clearer in Section VII, this has to do with interaction between the frequency sidebands, involving demodulation and interference effects.

Notably, in some cases such as the example shown in Fig. 2d, noise injection had the paradoxical effect of enhancing remote synchronization away from the injection site. This provides a compelling demonstration of the known possibility for weak additive noise to induce and enhance synchronization, in systems with both identical and non-identical units. In a system such as the present one where small parametric mismatches are present and structured synchronization patterns emerge, effectively obliterating a node generating activity that has primarily a repulsive effect with respect to the rest of the network can enhance synchronization, by means of lowering the energy transfer rate necessary to maintain a given level of synchrony between subsets of other nodes^{30,31}.

On another level, it remains unclear whether the present form of remote synchronization can or not act as a channel for “hidden” information propagation as previously speculated¹². In this regard, it is necessary to consider that even when information transfer is rigorously in-

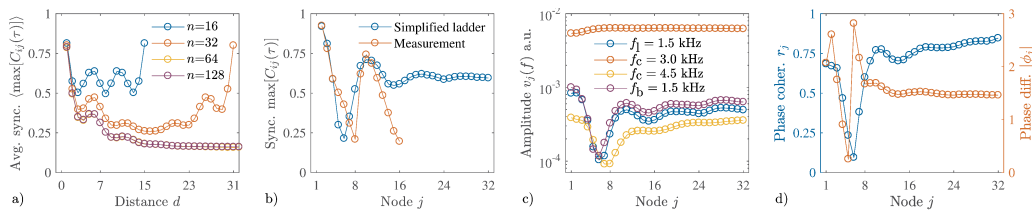


FIG. 3. Simulated rings and chain model. a) Average amplitude synchronization as a function of distance along the ring for simulated rings of different size. b) Amplitude synchronization measured experimentally along a ring segment (orange, calculated with respect to node $i = 1$ representing the input experimental time-series and truncated due to noise injection at node $j = 17$, see Fig. 2d), and corresponding simulated results from the simplified chain model (blue). c) Corresponding Fourier amplitudes of the predominant peak (f_c , orange, raw signal), lower and higher sidebands (f_l and f_h , blue and yellow, raw signal), and demodulated baseband (f_b , purple, signal envelope). d) Corresponding phase coherence and absolute phase shift between the lower sideband and demodulated baseband within each node j . See Sections V and VII for detailed description.

ferred in an observational framework, its detection cannot always be given a cause-effect interpretation unless specific conditions are met³², whereas intervening on the system through external perturbations elicits genuine causal effects and allows their evaluation in terms of *information flow*^{27,28}. This is exemplified by the hypothetical case of two neurons dissected together from brain tissue, which do not generate intrinsic activity but are structurally coupled to each other and therefore capable of exchanging externally-applied stimuli, implying that information transfer is zero but information flow is not.

Addressing this issue, experiments were performed injecting low-amplitude sinc pulses, setting $G_e = 1$ and a peak amplitude of ≈ 500 mV, corresponding to $\approx 1/3$ of the range of intrinsic activity; this allowed studying pulse propagation using a time-locked averaging approach while minimally disrupting the emergence of remote synchronization (Fig. 2e). We considered sinc pulses having a width of the main lobe of 0.5, 1 and 2 ms, corresponding approximately to 1.5, 3 and 6 times the inverse of the carrier frequency; corresponding run numbers for averaging were 65, 130 and 260. The peak value was extracted for each window, then compared to 100 random windows by means of a rank-order test, setting significance threshold to $\alpha = 0.05$. We observed that, in presence of remote synchronization of intrinsic activity, there was no remote propagation of these pulses, whose peak amplitude decayed rapidly and monotonically, disappearing into baseline after $d = 4$ steps (Fig. 2f); accordingly, even though the sinc pulses were clearly visible in the time-locked average at the injection site (Fig. 2g), they were completely undetectable at the distance corresponding to maximum remote synchronization (Fig. 2g).

Recalling that linear Granger causality clearly showed the remote effect (Fig. 1f), these results provide, from the perspective of linear interdependence, a compelling demonstration of decoupling between information flow (measured through intervention) and information transfer (measured by linear Granger causality). The mismatch is related to the fact that a linear model is inadequate for representing the dynamics of this system. Accordingly, the information flow resembled more closely information transfer as given by the non-linear and non-parametric analyses, however with a shorter range of propagation of the perturbation compared to information transfer of intrinsic activity (i.e. information transfer was still clearly detectable for $d \gg 4$ steps in Figs. 1g,h). All experimental time-series have been made publicly available³³.

V. DIFFERENT-SIZE RINGS AND SIMPLIFIED LADDER MODEL

To garner further confirmation of the local nature of the interactions supporting the emergence of remote synchronization, rings of different size $n = 16, 32, 64, 128$ (powers of

2 only for convenience, exact choice not relevant) were simulated as in Ref. 12, each one over 12 runs having random parametric mismatches ($\xi = 0.005$). The average amplitude synchronization was charted as a function of distance and exhibited a peak at $d \approx 6$, whose location was remarkably stable across runs and insensitive to ring size (Fig. 3a). Should the remote synchronization effect have been related to a global network phenomenon such as a collective oscillation mode, the location of the peak would plausibly have been sensitive to network size.

Further insight into the mechanisms underpinning remote synchronization can be obtained by considering a heavily simplified model, reproducing the phenomenon even without the ability to generate self-sustained oscillations and defined as follows. First, a open network is considered in the form of a chain, at the beginning of which an experimental signal is supplied as a source of predictive information; the signal from node $j = 1$ in Fig. 2d was chosen as this experiment yielded the most pronounced observation of remote synchronization, but the choice is not critical. Second, two dynamical equations are removed: the stage generating v_6 is replaced with a simple summer, and the integrator generating v_5 is removed altogether. Third, the non-linearity $\Gamma(x, y)$ is removed for all voltages except v_3 . Fourth, the parameters are set identically across all nodes, i.e. $\xi = 0$. One can then rewrite the system equations as

$$\begin{cases} \frac{dv_1}{dt} = 2\pi F(G_4 v_4 - v_1) \\ \frac{dv_2}{dt} = 2\pi F(G_1 v_1 - v_2) \\ \frac{dv_3}{dt} = \Gamma(K v_i, v_3) \\ \frac{dv_4}{dt} = 2\pi F(G_2 v_2 + G_3 v_3 - v_4) \end{cases} \quad (10)$$

where $v_o = G_5 v_1 + G_i v_i$. To reproduce remote synchronization, the parameters had to be slightly adjusted with a manual procedure which yielded $G_1 = -3.59$, $G_2 = -2.82$, $G_3 = -0.884$, $G_4 = -2.94$, $G_5 = 0.114$, $G_i = 0.604$, $F = 2$ kHz, $K = 0.091 \mu\text{s}^{-1}$ and $V_s = 4.7$ V. This model closely recovered the non-monotonic variation of amplitude synchronization with distance from the first node observed experimentally, dipping at node $j = 6$ and subsequently peaking at node $j = 10$, proving that closed network topology is not necessary for the emergence of remote synchronization (Fig. 3b). This model also demonstrated that, when an external signal is supplied as starting point, neither parametric mismatches, nor the second integrator nor multiple instances of the saturation non-linearity are necessary.

A difference with respect to the experimental system stands out: in simulations with the simplified model, after the initial spatial transient corresponding to the remote synchronization effect, the level of amplitude synchronization with respect to the initial signal stabilized at a relatively high level, i.e. $\max[C(\tau)] \approx 0.6$; by contrast, in the experimental system the synchronization rapidly decayed towards $\max[C(\tau)] \approx 0.2$ at $d \approx 16$.

To understand the underlying motivation, we next calculated conditional self-entropy in the simplified chain model and compared it to the full ring. Conditional self-entropy is akin to transfer entropy, but is obtained by swapping the roles of the past states of the target and driver: it quantifies the amount of information which is transferred internally within the target node, conditioning out the activity induced by the driver. It can therefore be viewed as a measure of the extent to which a node is an ‘‘active’’ signal generator as opposed to a ‘‘passive’’ entity simply relaying the input signal, albeit with a potentially non-linear transformation³⁴. We observed that the conditional self-entropy in the simplified chain model peaked at node $j = 4$ with $S_{4|3} = 0.14$ and thereafter gradually decreased along the chain until $S_{32|31} = 0.03$, being overall substantially lower compared to the full ring in the chaotic state, i.e. 0.03 ± 0.02 vs. 0.33 ± 0.08 , $p < 0.001$.

This reveals that although the simplified model can closely reproduce the remote synchronization effect when fed an experimental time-series as a source of predictive information

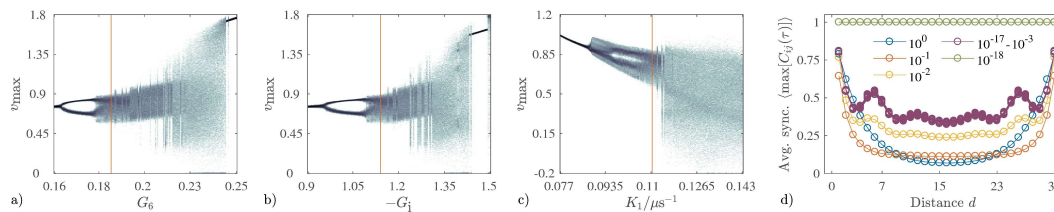


FIG. 4. Control parameter sweep and mismatch level simulations. a), b) and c) Bifurcation diagrams showing the local maxima distribution as a function of the control parameters G_6 , G_i and K_1 , revealing transition to chaos and subsequent crisis. Red bars denote parameter settings chosen for observing remote synchronization, logarithmic gray-scale. d) Average amplitude synchronization as a function of distance along the ring, delineating the basin of attraction of the remotely-synchronized state (purple plot, peak at $d = 6$) as a function of the parameter mismatch level. See Section VI for detailed description.

at the beginning of the chain, crucially its nodes are, at least to a large extent, not “active” signal generators, meaning that they do not generate predictive information independently of that received from the other connected nodes. It is for this reason that, after the initial transient, the level of synchronization with respect to the initial time series remains high: in the full system, each node acts as a source of predictive information and thus generates an own signal which is overlapped to the input signal, and therefore after the initial spatial transient a synchronization decay is observed owing to diffusion. In turn this finding indicates that in the full system the non-linearity plays two distinct roles. One is generative, namely supporting chaotic dynamics. The other, as will be clarified below, consists of enabling energy transfer between the frequency bands; in this simplified model, the non-linearity largely or solely plays the latter role, and it is for this reason that parametric mismatches are not necessary, whereas in the full model some repulsion is required to avoid entering the globally-synchronized state.

VI. TRANSITIONS AND EFFECT OF PARAMETRIC MISMATCHES

Prior to revealing the cross-frequency interaction giving rise to remote synchronization, it is appropriate to confirm that the underlying dynamics are indeed chaotic. As reported in Ref. 12, three dynamical regimes featuring different frequency spectra are observed as a function of the control parameter settings in this system: quasiperiodicity, “fully-developed” chaos and a form of “weaker” chaos. These were characterized, respectively, by a comb-like spectrum of delta functions, a broadband spectrum without distinct peaks, and an intermediate spectrum with narrow peaks, broader than delta functions but well-separated. Remote synchronization was observed only for the third case, which is close to quasiperiodicity and wherein chaoticity was manifest in the form of relatively constrained amplitude fluctuations. Since in Ref. 12 route-to-chaos analysis was not performed and the largest Lyapunov’s exponent was not calculated, there remains the question whether the system is truly chaotic in such state, or the corresponding broad peaks more trivially reflect the parametric mismatches.

To address this issue, simulations were performed for a ring of $n = 32$ nodes, sweeping the control parameters G_6 , G_i and K_1 and generating bifurcation diagrams from the local maxima; as in Ref. 12, for observing remote synchronization in the simulations we set $G_6 = 0.188$ and $G_i = -1.14$, and separately swept $G_6 \in [0.16, 0.25]$ (Fig. 4a), $-G_i \in [0.9, 1.5]$ (Fig. 4b) and $K_1 \in [0.077, 0.143] \mu s^{-1}$ (Fig. 4c). As a function of all three control parameters, period doubling and subsequent transition to chaos were clearly observed, followed by a sudden change in the size of the chaotic attractor, also known as an interior crisis^{17,35}. The corresponding largest Lyapunov exponent λ_{\max} was estimated using Kantz’s method ($\Delta t = 1 \mu s$, 250,000 pts.)³⁶. Prior to the crisis, i.e. for the regime associated with remote

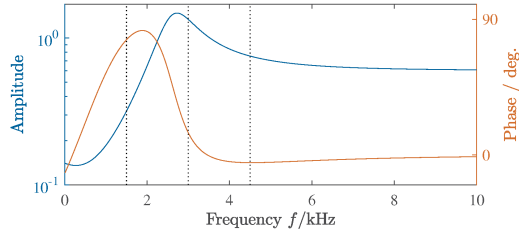


FIG. 5. Amplitude and phase responses of each node according to the simplified model in Eq. (10), rendered linear time-invariant by disregarding the integrator and associated non-linearity, i.e. setting $G_3 = 0$. Dashed lines denote the locations of $f_1 = 1.5$ kHz, $f_c = 3.0$ kHz and $f_h = 4.5$ kHz. See Section VII for detailed description.

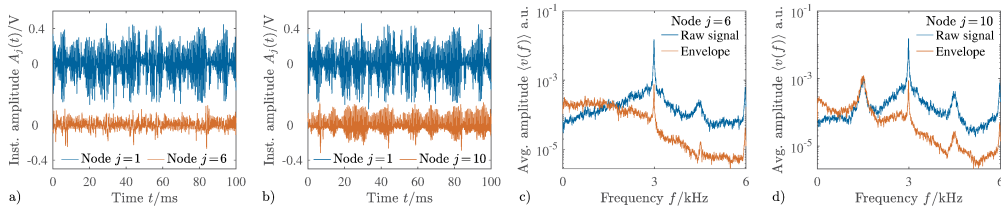


FIG. 6. Representative time-series and spectra from the simplified model. a) and b) Instantaneous amplitudes, comparing the activity in node $j = 1$ to that in nodes $j = 6, 10$, representing the synchronization dip and subsequent recovery. Mean voltage has been subtracted. c) and d) Corresponding frequency spectra for the raw signals and envelopes. See Sections V and VII for detailed description.

synchronization ($G_6 = 0.188$, $G_i = -1.14$), we measured $\lambda_{\max} = 0.0032 \pm 0.0004$, whereas after the crisis, i.e. for the regime yielding the continuous frequency spectrum spectrum ($G_6 = 0.196$, $G_i = -1.365$), we measured $\lambda_{\max} = 0.0045 \pm 0.0008$.

These results confirm that when remote synchronization is observed in this system the underlying dynamics are indeed chaotic, however there remains the question of what influence the presence of parametric mismatches has on the emergence of this state. To address this issue, additional simulations were performed sweeping $\xi \in [10^{-18}, 10^0]$ (Fig. 4d). We observed that for $\xi \in [10^{-17}, 10^{-3}]$, remote synchronization reliably emerges with negligible dependence on ξ . Contrariwise, for $\xi \leq 10^{-18}$ and $\xi \geq 10^{-2}$ two qualitatively different states are observed, respectively characterized by global synchronization and partial synchronization without remoteness (i.e. monotonic synchronization decay with distance). This indicates that, even though the state of remote synchronization has a large basin of attraction, three states actually coexist³⁷. Parametric mismatches are therefore necessary to provide some level of repulsion allowing activity to become differentiated across nodes, but when they are too large they overwhelm the non-linear mechanism of energy exchange between frequency bands underlying the effect (see Section V), and simpler synchronization phenomena prevail³⁰. It is noted that the tolerances estimated for the physical system, i.e. $\xi = 0.005$, are close to the upper bound for which remote synchronization emerges. More generally, remote synchronization requires parameter settings sustaining the interference effect reported in Section VII, where global synchronization and partial synchronization without remoteness arise over extended regions. Sharp transitions between the three states can be observed particularly as a function of gains G_2 and G_3 (data not shown).

VII. DEMODULATION AND INTERFERENCE

Having established that remote synchronization is a local effect by means of noise perturbation experiments together with simulations on rings of different size and the simplified

chain model, it shall now be demonstrated that the underlying phenomenon consists of a form of cross-frequency interaction. In simulations of the simplified model, the central, lower and higher peaks introduced in Section II are found at $f_c = 3.0$ kHz, $f_l = 1.5$ kHz and $f_h = 4.5$ kHz respectively. The central peak is predominant and reflects oscillation periodicity. As previously stated, the lower peak at frequency $f_l = f_c/2$ hallmarks anti-persistent dynamics, stemming from an underlying period-doubling bifurcation, whereas the higher peak corresponds to its image frequency with respect to the central peak, $f_h = f_l + f_c$. Since the central peak is predominant and the weaker sidebands are symmetric with respect to it, the spectrum recalls that of standard amplitude modulation (AM) with carrier frequency f_c and baseband signal at frequency $f_b = f_c - f_l = f_h - f_c$. However, unlike typical applications of AM techniques, the relationship $f_h = f_l + f_c$ is simultaneously verified, implying that the lower sideband and the baseband are spectrally coincident, which is only possible if $f_l = f_b = f_c/2$. This situation quite commonly arises in chaotic systems that have anti-persistent dynamics but is not found, for example, whenever chaoticity follows non-linear interaction between oscillations at unrelated frequencies; examples of both scenarios can be found among transistor-based chaotic oscillator circuits^{17,38}.

This specific spectral configuration is however plausibly not a necessary condition for the emergence of forms of remote synchronization such as the present one, since interference between preexisting and demodulated baseband signal as described below could in principle also arise with $f_l \neq f_b$; it is also not a sufficient condition because in the present system it is observed over wide ranges of parameter settings, including regions without remote synchronization (data not shown). Notably, amplitude modulation has previously been considered as a possible means of information transmission in chaotic networks, however in a different framework³⁹.

In the simplified chain model described in Section V, while the amplitude of the central peak remained relatively constant along the chain, the amplitudes of the sidebands underwent large spatial fluctuations. Namely, the synchronization dip at node $j = 6$ (Fig. 3b) was associated with partial cancellation particularly of the lower sideband, followed by recovery showing damped spatial oscillation, and resembling a diffraction pattern (Fig. 3c).

To elucidate the mechanism underlying interference, it is necessary to consider more closely the properties of each node (Eq. (1) and Fig. 1a for the full system; Eq. (10) for the simplified model). In particular it is useful to consider the response of the simplified model, further simplified and rendered linear time-invariant by neglecting the integrator and associated saturation non-linearity, i.e. setting $G_3 = 0$. Due to the ring structure, formed of the three composite stages implementing gain and low-pass filtering and realizing a resonator, and summation of their output to the input from the previous node, for the chosen parameter settings each node has frequency and phase responses which resemble a peaking filter at low frequencies and a simple pass-through at high frequencies. As such, this arrangement emphasizes the higher sideband relative to the lower one, which it significantly attenuates and dephases (Fig. 5). Due to presence of the integrator(s) and associated saturation non-linearity, another signal component in the frequency range of the lower sideband is concomitantly generated. In particular, because saturation occurs in a highly asymmetric manner, the non-linearity effectively realizes an envelope detector, resembling the demodulation mechanism found in early AM radio receivers. In fact, further simplifying the non-linearity so that it includes only negative saturation

$$\Gamma(x, y) = R(x) - R(-x)H(V_s + y) \quad (11)$$

the close overlap between experimental data and the chain model can still be perfectly reproduced (Fig. 3b). Depending on the phase relationship between the low-frequency component preexistent in the input signal and such demodulated signal, constructive or destructive interference can arise; this in turn also reflects in the higher sideband, but to a lesser extent since the non-linearity has primarily a demodulating action.

The fact that in the simplified chain model each node acts as a relay without overlapping an own chaotic signal facilitates demonstrating how the “hidden” baseband signal (amplitude fluctuations) can easily be recovered. For example, considering a second-order peaking filter having manually chosen $f_0 = 4.425$ kHz and $Q = 4.5$, and calculating amplitude

synchronization based on the envelope of the signal thus filtered, the dip in synchronization with respect to the initial signal is drastically attenuated, with corresponding dip $\max[C(\tau)] = 0.55$ at node $j = 8$ as opposed to $\max[C(\tau)] = 0.20$ at node $j = 6$, rendering the synchronization of more distant nodes no longer remote. To recover the “hidden” signal it is therefore sufficient to perform a linear operation, namely attenuate the lower sideband and emphasize the higher sideband, and then obtain the baseband signal by demodulation, that is, envelope detection. However, non-linearity is necessary to obtain the non-monotonic spatial relationship underlying remote synchronization.

To further clarify the manner in which the synchronization dip appears at a certain distance, it is helpful to consider the spatial variation along the chain of the phase relationship between the lower sideband and the demodulated baseband within each node, which for explanatory purpose we simply recover via the same peaking filter. Such spatial variation stems from the master-slave coupling architecture, which cascades the responses and dynamics of the nodes. The phase coherence between the lower sideband and demodulated baseband r_j dipped at node $j = 6$, corresponding to the point of maximally destructive interference, then raised again, peaking at node $j = 10$ (Fig. 3d). Consideration of the absolute phase shift $|\phi_j|$ further indicated that the relationship between the lower sideband and demodulated baseband rapidly drifted at the beginning of the chain, until a stable phase shift was attained after node $j = 8$ (Fig. 3d). The non-monotonic changes of synchronization observed in the simplified chain model, as well as in the full ring, are therefore underpinned by the phase shift between the lower sideband and the demodulated baseband, which is initially spatially unstable and at a certain distance leads to almost complete cancellation. This distance depends in a non-trivial manner on the system parameters, particularly filter frequency F (data not shown). The carrier and higher sideband are sufficiently preserved, and the low frequency signal is eventually recovered from them (Fig. 6a-d).

This account of the remote synchronization mechanism can be corroborated through directly intervening in the simplified chain model by instancing filters selectively attenuating either sideband. Additional simulations were therefore performed adding at specified sites either a high-pass filter having $f_{\text{stop}} = 1.5$ kHz and $f_{\text{pass}} = 2.0$ kHz (only removing the lower sideband), or a low-pass filter having $f_{\text{pass}} = 4.0$ kHz and $f_{\text{stop}} = 4.5$ kHz (only removing the higher sideband); in both cases, finite impulse response (FIR) equiripple filters with passband ripple 1 dB, stop-band attenuation 40 dB were used (Fig. 7a). First, we instanced the filters before the synchronization dip, at node $j = 3$. As expected for an interference effect, removing either sideband, particularly the lower one, attenuated the dip; furthermore, removing the higher sideband introduced a shallower desynchronization peak further down the chain around nodes 10-12 (Fig. 7b). Second, we instanced the filters at the site corresponding to the synchronization dip, namely at node $j = 6$. Here, a striking difference was observed between the effect of removing the lower or higher sideband: while removing the lower sideband had negligible effect on the recovery of synchronization further down the chain (0.60 ± 0.02 vs. 0.60 ± 0.02 , $p = 0.6$), removing the higher sideband effectively obliterated it (0.20 ± 0.04 vs. 0.60 ± 0.02 , $p < 0.001$; Fig. 7c). Third, we instanced the filters just two steps further down the chain, at node $j = 8$, observing a totally different effect, whereby removing the higher sideband did not impair the eventual recovery of synchronization but only engendered a new interference dip around node $j = 16$ (Fig. 7d). Although partially dependent on the filter choices (data not shown), these interventions confirm the occurrence of significant energy exchange between the frequency sidebands and subsequent interference, and more specifically reveal that at the point of synchronization dip, the “hidden” synchronization information is conveyed predominantly through the higher sideband and carrier signal.

VIII. REVISED GRANGER CAUSALITY ANALYSIS

In the simplified chain model, it was shown that synchronization dips at a certain distance from a starting node due to destructive interference between the lower sideband (low

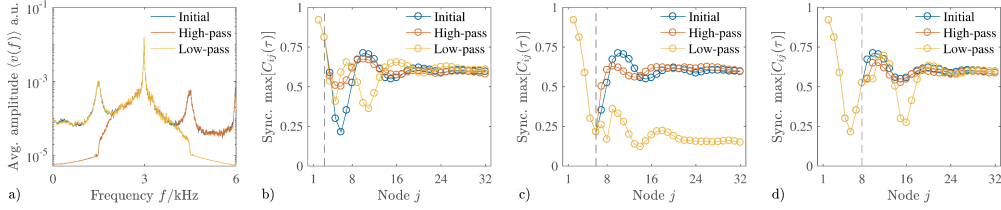


FIG. 7. Intervention consisting of blocking out either sideband in the simplified model. a) Average frequency spectra of the initial, low- and high-pass filtered signals (blue, yellow, orange). b), c) and d) Effect of inserting the corresponding low- and high-pass filters along the chain model after nodes $j = 3, 6, 8$. See Sections V and VII for detailed description.

frequency activity preexisting in the input signal) and the demodulated baseband (generated locally), which almost completely cancels out the amplitude fluctuations (envelope) for which remote synchronization is observed in this system. Importantly, in the full ring each node acts not only as a relay but also as an “active” generator of an own signal, therefore such effect is found in a “staggered” arrangement, wherein each node simultaneously processes the signals from multiple previous nodes located at different distances. This turns the synchronization dip and subsequent recovery observed for the chain model (Fig. 3b) into the diagonal pattern visible to both correlation and linearity analyses (Fig. 1e,f).

Having established that the lower sideband and baseband are spectrally coincident, extracting the former via low-pass filtering should reveal correlation and causality patterns reflecting the results originally obtained for amplitude fluctuations, determined using Hilbert’s transform as detailed in Section II. To verify this hypothesis, the signals from the initial experiments were processed through a low-pass FIR filter having $f_{\text{pass}} = 2.0$ kHz and $f_{\text{stop}} = 2.5$ kHz, passband ripple 0.1 dB, stopband attenuation 40 dB (Fig. 8a); in order not to confound causality in these analyses, zero-phase digital filtering was performed (leading to squared transfer function and doubled filter order). While filtering to isolate causal influences within specific frequency bands can be problematic^{40,41} and is theoretically unnecessary⁴⁰, for the present purpose it was deemed appropriate since there was a strong prior to confirm the previous analysis and need to prevent the much stronger carrier frequency from overwhelming the low-frequency dynamics. For consistency, the same settings as in Section III were kept, namely $\tau = 0.18$ ms and $p = 16$. As expected, applying the Granger linear model in Eq. (7) to the resulting signal yielded a causality pattern closely resembling the one previously obtained for the envelope signal (Fig. 8b).

In the simplified chain model, at the point of synchronization dip the “hidden” synchronization information could be recovered by applying a peaking filter to emphasize the higher sideband and carrier with respect to the lower sideband, and then extracting the envelope. This is because, as also confirmed by simulations on the insertion of filters in the chain, at that point the synchronization information is conveyed predominantly through the higher sideband, since the lower sideband is almost completely nulled. It should therefore be possible to apply a similar approach to “plug” the diagonal line of desynchronization observed in the full ring. For this purpose, the initial experimental signals were filtered using a second-order peaking filter having manually chosen $f_0 = 3.65$ kHz and $Q = 3$ (Fig. 8a), and the envelope of this signal was considered. In the resulting causality pattern, remoteness was considerably less evident and the information transfer more closely followed a monotonic decay (Fig. 8c).

Even though destructive interference primarily affected the lower sideband so that more predictive information was conveyed by the higher sideband, due to the non-linearity there is a mutual interdependence between the two, which in the full ring is further complicated by the “active” role of each node. It is therefore reasonable to speculate that the lower sideband signals may contain predictive information not present in the higher sideband signals. Exploring this possibility, a final analysis was conducted simultaneously including into the regressors the activity of both sidebands. The resulting causality matrix revealed markedly

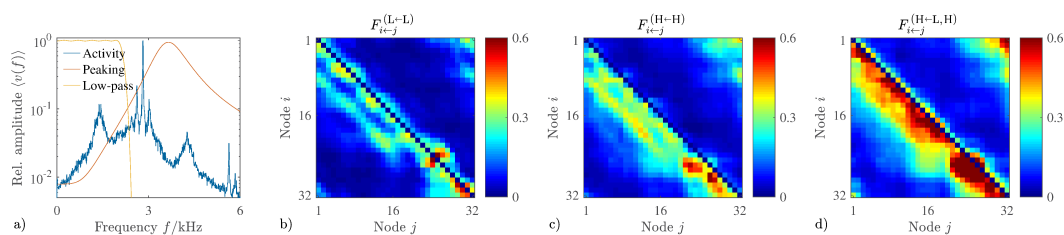


FIG. 8. Granger causality analyses for the lower sideband (L) and baseband demodulated from the filtered higher sideband (H). a) Average frequency spectrum of the experimentally-measured signals (normalized to unit maximum), and amplitude responses of the chosen low-pass and peaking filters. b) Granger causality for the lower sideband. c) Granger causality for the demodulated baseband, i.e. envelope of the higher sideband extracted via the peaking filter. d) Granger causality according to a model merging the predictors considered in b) and c). Raw signals from Ref. 12. See Section VIII for detailed description.

stronger information transfer, without any residual aspect of remoteness (Fig. 8d). Taken together, these findings demonstrate that a linear causality model is capable of resolving the underlying information transfer, insofar as the activity of both sidebands is represented in a manner appropriate for the system, in this case through filtering and demodulating the higher sideband. This is the relationship which could be approximated by the quadratic Granger model and agnostically captured by the model-free transfer entropy analysis reported in Section III.

IX. DISCUSSION

In Ref. 12, an instance of morphogenesis was reported wherein complex synchronization networks, having small-world features, emerge from ring structural connectivity primarily via remote and cluster synchronization of amplitude fluctuations. Here, such phenomenological account is extended via a comprehensive set of additional experiments and simulations, which finally elucidate the underlying mechanism.

First, by explicitly considering information transfer in addition to synchronization, it was confirmed that the patterns which are formed truly reflect causal interdependence, which appears to be remote insofar as simple linear causality models are considered. It was also confirmed that these patterns arise for chaotic dynamics in a region featuring a power spectrum with broad but clearly separate peaks, and denote a state with a large basin of attraction, such that small parametric mismatches between the nodes provide sufficient repulsion to avoid entering global synchronization.

Second, through lesioning the experimental system via localized injections of noise, as well as simulations varying the network size and opening the ring, it was demonstrated that the pattern formation effect has local nature, meaning that rather than reflecting a collective behavior of the entire network it arises primarily from the interactions between each node and its surroundings.

Third, using a simplified chain model wherein each node purely acts as a relay without generating an own chaotic signal, it was shown that amplitude fluctuations become desynchronized at a certain distance from a starting node, due to a destructive interference effect arising between low-frequency activity that is preexisting in the signal and locally demodulated from other frequency bands. It was understood that a spatially-dependent phase relationship between such signals leads to a synchronization dip at a certain distance, beyond which entrained fluctuations are recovered from synchronization information conveyed in a modulated form at higher frequencies; this hypothesis was also confirmed via interventions consisting of instancing filters at different locations along the chain.

Fourth, it was clarified that such form of cross-frequency interaction is the relationship that is captured by generalized synchronization measures and model-free causality analyses,

which in this and the previous study revealed a gradient without aspects of remoteness¹². This reconciles the observations of information transfer with those of information flow, which did not detect any remote propagation of external perturbations.

These observations strongly exemplify how divergent results on the topology of the emergent synchronization and causality networks may be obtained depending on whether linear vs. non-linear or model-free approaches are considered. The notion of remote synchronization is in itself one that needs to be considered in the well-defined context of a specific synchronization measure. From the perspective of amplitude synchronization, intended as linear correlation or phase coherence of amplitude fluctuations, the present system unquestionably exhibits remote synchronization. However, from the perspective of generalized synchronization, which arguably represents a weaker form of entrainment, there is no remoteness³⁰. Notably, this is also true for the related phenomenon of relay synchronization observed in Rössler oscillator networks, wherein measures of generalized synchronization readily reveal the mechanism of entrainment, and thus the presence of partial synchronization gradients¹¹. Importantly, the same situation is found for information transfer: it appears remote only when assessed via linear causality models, the invalidity of which is, in the present case, already manifest during model order selection. As soon as models tailored to account for the specific behavior of the system or model-free approaches are applied, it becomes evident that the statistical interdependence between nodes is not truly remote.

Finally, the generality of the phenomenon should be addressed. The observed form of remote synchronization does not require a cyclic topology and may arise in any network containing a chain motif. Since this effectively corresponds to the totality of known complex networks, future work should extend the present findings to complex topologies, thus addressing the potential relevance of this phenomenon to collective behaviors in more naturalistic scenarios, as previously done for remote synchronization in Stuart-Landau systems⁴.

As observed in other physical systems such as plasmas⁴², any suitable non-linearity can engender a demodulating effect, hence there is no unique relevance of the saturation non-linearity present at the integrator outputs. However, in order for an interference effect to support pattern formation in the way we have observed, it is necessary for a chaotic signal to feature distinct peaks on the power spectrum, having frequency relationships such that activity at one or more frequencies can constructively or destructively interfere with that at other frequencies, through demodulation with respect to a carrier signal. Such requirement is met for example whenever the strongest peaks are located at frequencies Ω_1 , Ω_2 and $\Omega_1 - \Omega_2$, but may not be met whenever chaos arises via the quasiperiodicity route from unrelated frequencies^{17,38}.

As indicated by earlier observations in Ref. 12, interference is therefore plausibly unable to engender remote synchronization whenever the spectrum is broadband, that is, devoid of distinct peaks. Power spectral features are more closely related to the mixing properties of strange attractors than to system characteristics, and depending on the region the majority of chaotic systems can generate both broadband signals or power spectra with narrow peaks, as exemplified by the band and funnel attractors in the Rössler system⁴³. Even though putatively self-organized critical systems such as the brain tend to generate broadband signals, this does not exclude the possibility of observing narrower spectra, and consequently interference, at the microscopic scale⁴⁴. The observed interference effect recalls two-tone interference in hearing, in particular in its manifestation as two-tone suppression⁴⁵. Furthermore amplitude modulation and interference effects have previously surfaced in models of asynchronous neuronal populations closely fitting extracellular recordings⁴⁶. More generally the importance of cross-frequency coupling effects in neural systems is only recently being considered, and it is plausible that complex pattern formation mechanisms such as the one observed in the present study may also underpin the mismatch observed between entrainment of spontaneous activity and responses to external perturbations^{47,48}.

Last, the spatial phase gradient leading to interference at a specific location can only be maintained in the context of unidirectional coupling and would be dissipated under diffusive coupling, rendering the observed phenomenon pertinent specifically for directed networks.

ACKNOWLEDGMENTS

All experimental activities were self-funded by L.M. personally and conducted on own premises.

- ¹A. Arenas, A. Díaz-Guilera, J. Kurths, Y. Moreno and C. Zhou, *Synchronization in complex networks*, Phys. Rep. **469** (2008) (3), pp. 93–153
- ²L. Pecora, F. Sorrentino, A. Hagerstrom, T. Murphy and R. Roy, *Cluster synchronization and isolated desynchronization in complex networks with symmetries.*, Nat. Commun. **5** (2014), p. 4079
- ³I. Fischer, R. Vicente, J. M. Buldú, M. Peil, C. R. Mirasso, M. Torrent and J. García-Ojalvo, *Zero-lag long-range synchronization via dynamical relaying*, Phys. Rev. Lett. **97** (2006) (12), p. 123902
- ⁴L. V. Gambuzza, M. Frasca, L. Fortuna and S. Boccaletti, *Inhomogeneity induces relay synchronization in complex networks*, Phys. Rev. E **93** (2016) (4), p. 042203
- ⁵D. M. Abrams and S. H. Strogatz, *Chimera states for coupled oscillators*, Phys. Rev. Lett. **93** (2004) (17), p. 174102
- ⁶M. J. Panaggio and D. M. Abrams, *Chimera states: coexistence of coherence and incoherence in networks of coupled oscillators*, Nonlinearity **28** (2015) (3), p. R67
- ⁷A. Bergner, M. Frasca, G. Sciuto, A. Buscarino, E. J. Ngamga, L. Fortuna and J. Kurths, *Remote synchronization in star networks*, Phys. Rev. E **85** (2012) (2), p. 026208
- ⁸L. V. Gambuzza, A. Cardillo, A. Fiasconaro, L. Fortuna, J. Gómez-Gardenes and M. Frasca, *Analysis of remote synchronization in complex networks*, Chaos **23** (2013) (4), p. 043103
- ⁹V. Nicosia, M. Valencia, M. Chavez, A. Díaz-Guilera and V. Latora, *Remote synchronization reveals network symmetries and functional modules*, Phys. Rev. Lett. **110** (2013) (17), p. 174102
- ¹⁰L. Zhang, A. E. Motter and T. Nishikawa, *Incoherence-Mediated Remote Synchronization*, Phys. Rev. Lett. **118** (2017) (17), p. 174102
- ¹¹R. Gutiérrez, R. Sevilla-Escoboza, P. Piedrahita, C. Finke, U. Feudel, J. M. Buldu, G. Huerta-Cuellar, R. Jaimes-Reategui, Y. Moreno and S. Boccaletti, *Generalized synchronization in relay systems with instantaneous coupling*, Phys. Rev. E **88** (2013) (5), p. 052908
- ¹²L. Minati, *Remote synchronization of amplitudes across an experimental ring of non-linear oscillators*, Chaos **25** (2015) (12), p. 123107
- ¹³E. Ihlen, *Introduction to Multifractal Detrended Fluctuation Analysis in Matlab*, Front Physiol. **3** (2012), p. 141
- ¹⁴B. Boashash, *Estimating and interpreting the instantaneous frequency of a signal. II. Algorithms and applications*, Proc. IEEE **80** (1992) (4), pp. 540–568
- ¹⁵T. Schreiber, *Measuring information transfer*, Phys. Rev. Lett. **85** (2000) (2), p. 461
- ¹⁶R. Vicente, M. Wibral, M. Lindner and G. Pipa, *Transfer entropy a model-free measure of effective connectivity for the neurosciences*, J. Comput. Neurosci. **30** (2011) (1), pp. 45–67
- ¹⁷E. Ott, *Chaos in Dynamical Systems* (Cambridge University Press, 2002)
- ¹⁸J. T. Lizier, M. Prokopenko and A. Y. Zomaya, *Local measures of information storage in complex distributed computation*, Inf. Sci. **208** (2012), pp. 39–54
- ¹⁹C. W. Granger, *Investigating causal relations by econometric models and cross-spectral methods*, Econometrica (1969), pp. 424–438
- ²⁰J. Geweke, *Measurement of linear dependence and feedback between multiple time series*, J. Am. Stat. Assoc. **77** (1982) (378), pp. 304–313
- ²¹A. M. Fraser and H. L. Swinney, *Independent coordinates for strange attractors from mutual information*, Phys. Rev. A **33** (1986), pp. 1134–1140
- ²²E. J. Ward, *A review and comparison of four commonly used Bayesian and maximum likelihood model selection tools*, Ecol Modell. **211** (2008) (1), pp. 1 – 10
- ²³L. Faes, G. Nollo and K. H. Chon, *Assessment of Granger causality by nonlinear model identification: application to short-term cardiovascular variability*, Ann Biomed Eng. **36** (2008) (3), pp. 381–395
- ²⁴A. Kraskov, H. Stögbauer and P. Grassberger, *Estimating mutual information*, Phys. Rev. E **69** (2004) (6), p. 066138
- ²⁵L. Faes, D. Kugiumtzis, G. Nollo, F. Jurysta and D. Marinazzo, *Estimating the decomposition of predictive information in multivariate systems*, Phys. Rev. E **91** (2015), p. 032904
- ²⁶L. Barnett, A. B. Barrett and A. K. Seth, *Granger Causality and Transfer Entropy Are Equivalent for Gaussian Variables*, Phys. Rev. Lett. **103** (2009), p. 238701
- ²⁷J. Pearl, *Causality: Models, Reasoning and Inference*, 2nd ed. (Cambridge University Press, New York, NY, USA, 2009)
- ²⁸J. T. Lizier and M. Prokopenko, *Differentiating information transfer and causal effect*, Eur. Phys. J. B. **73** (2010) (4), pp. 605–615
- ²⁹J. Teramae and Y. Kuramoto, *Strong desynchronizing effects of weak noise in globally coupled systems*, Phys. Rev. E **63** (2001), p. 036210
- ³⁰S. Boccaletti, J. Kurths, G. Osipov, D. Valladares and C. Zhou, *The synchronization of chaotic systems*, Phys. Rep. **366** (2002) (1), pp. 1 – 101
- ³¹J. Teramae and D. Tanaka, *Robustness of the Noise-Induced Phase Synchronization in a General Class of Limit Cycle Oscillators*, Phys. Rev. Lett. **93** (2004), p. 204103

- ³²D. Chicharro and A. Ledberg, *When Two Become One: The Limits of Causality Analysis of Brain Dynamics*, PLoS ONE **7** (2012) (3), pp. 1–16
- ³³*Experimental perturbation time-series available at*, <http://www.lminati.it/listing/2018/a/>
- ³⁴L. Faes, A. Porta and G. Nollo, *Information Decomposition in Bivariate Systems: Theory and Application to Cardiorespiratory Dynamics*, Entropy **17** (2015) (1), pp. 277–303
- ³⁵C. Grebogi, E. Ott and J. A. Yorke, *Crises, sudden changes in chaotic attractors, and transient chaos*, Physica D. **7** (1983) (1), pp. 181 – 200
- ³⁶H. Kantz, *A robust method to estimate the maximal Lyapunov exponent of a time series*, Phys. Lett. **185** (1994) (1), pp. 77 – 87
- ³⁷P. J. Menck, J. Heitzig, N. Marwan and J. Kurths, *How basin stability complements the linear-stability paradigm*, Nat. Phys. **9** (2013), pp. 89 – 92
- ³⁸L. Minati, M. Frasca, P. Oświecimka, L. Faes and S. Drożdż, *Atypical transistor-based chaotic oscillators: Design, realization, and diversity*, Chaos **27** (2017) (7), p. 073113
- ³⁹B. Cessac and J. A. Sepulchre, *Transmitting a signal by amplitude modulation in a chaotic network*, Chaos **16** (2006) (1), p. 013104
- ⁴⁰L. Barnett and A. Seth, *Behaviour of Granger causality under filtering: Theoretical invariance and practical application*, J. Neurosci. Methods **201** (2011) (2), pp. 404–419
- ⁴¹E. Florin, J. Gross, J. Pfeifer, G. R. Fink and L. Timmermann, *The effect of filtering on Granger causality based multivariate causality measures*, NeuroImage **50** (2010) (2), pp. 577 – 588
- ⁴²M. Sodha, A. K. Arora and A. K. Aggarwal, *Nonlinear Demodulation of an Amplitude Modulated Wave in a Plasma: Elementary Approach*, Radio Sci. **3** (1968) (12), pp. 1124–1131
- ⁴³D. Farmer, J. Crutchfield, H. Froehling, N. Packard and R. Shaw, *Power spectra and mixing properties of strange attractors*, Ann. N. Y. Acad. Sci. **357** (1980) (1), pp. 453–471
- ⁴⁴B. J. He, *Scale-free brain activity: past, present, and future*, Trends Cogn Sci. **18** (2014) (9), pp. 480 – 487
- ⁴⁵F. Jülicher, D. Andor and T. Duke, *Physical basis of two-tone interference in hearing*, Proc. Natl. Acad. Sci. U.S.A. **98** (2001) (16), pp. 9080–9085
- ⁴⁶J. Díaz, P. Razeto-Barry, J.-C. Letelier, J. Caprio and J. Bacigalupo, *Amplitude Modulation Patterns of Local Field Potentials Reveal Asynchronous Neuronal Populations*, J. Neurosci. **27** (2007) (34), pp. 9238–9245
- ⁴⁷V. Jirsa and V. Mller, *Cross-frequency coupling in real and virtual brain networks*, Front Comput Neurosci. **7** (2013), p. 78
- ⁴⁸M. Bortoletto, D. Veniero, G. Thut and C. Miniussi, *The contribution of TMS-EEG coregistration in the exploration of the human cortical connectome*, Neurosci. Biobehav. Rev. **49** (2015), pp. 114 – 124